International Journal of QUANTUM CHEMISTRY

Atmospheric Degradation Mechanisms of a Simulant Organophosphorus Pesticide Isopropyl Methyl Methylphosphonate: A Theoretical Consideration

Shu-Xian Hu,[a,b] Jian-Guo Yu,*[c] and Eddy Y. Zeng[a]

Calculations using density functional theory were performed to explore the mechanisms for atmospheric degradation of isopropyl methyl methylphosphonate (IMMP). The potential energy surface profiles for OH-initiated reaction of IMMP were constructed, and all possible degradation channels were considered. Rate constants were further calculated using transition state theory. It was established from these calculations that H-abstractions from alkyl groups have much lower energy barriers than substitutions of alkoxyl groups, and four possible H-abstraction channels are competitive. Investigations into the secondary reactions under the presence of O_2/NO were also performed. It is shown that O_2 addition, reaction of peroxide radicals with NO to form RO radicals, and removal of ·RO are the major degradation pathways for alkyl radicals. Four selected products, $CH_3OP(O)(CH_3)OC(O)CH_3$, $CH_3OP(O)(O)CH_3$, $(CH_3)_2CHOP(O)(CH_3)OH$, and $(CH_3)_2CHOP(O)(CH_3)OCH{=}O$, are predicted to be the major products in this study. © 2012 Wiley Periodicals, Inc.

DOI: 10.1002/qua.24182

Introduction

In recent years, global consumption of organophosphorus compounds (OPs) has increased sharply. Apart from being used as synthetic insecticides in agriculture and household pest control,[1–4] OPs are also applied as chemical warfare agents.[5,6] Primary removal routes of OPs are by wet and dry depositions, and by chemical reactions occurring during long-range transport to remote regions.[2,7–9] They are highly toxic not only toward a variety of aquatic organisms, birds, insects and pests but also toward exposed human population via inhalation, dermal contact, and ingestion.[4,6,10]

Experimental studies suggested that OPs introduced into the troposphere are subsequently removed by chemical reaction, dominantly with OH radicals.[1,2,9,11–17] Previous experimental and theoretical studies on OPs containing —OCH_3 or —OCH_2— reported that reactions of these OPs with O_2/NO result in the formation of an alkoxy radical (>P(O)OCH(O·)—).[12,15,18–22] These results are in agreement with a subsequent rearrangement of the alkoxy radical occurring through a five-member transition state with the formation of >P(O)OH and a molecular carbonyl radical. In a recent experimental study,[23] the rate constant for atmospheric reaction of OH radicals and a simulant OP containing the —OCH< and —OCH_3 groups isopropyl methyl methylphosphonate (IMMP, $(CH_3)_2CHOP(O)(CH_3)OCH_3$) was determined to be 6.72×10^{-11} cm^3 mol^{-1} s^{-1} at 298 K. The major initial product observed was $CH_3OP(O)(CH_3)OC(O)CH_3$, while a number of additional ion peaks were observed, which were all attributed to secondary products.

This study is the first to elucidate the degradation mechanisms for OH-initiated oxidation reactions of IMMP in the presence of O_2/NO. In addition, the reaction free energy, barrier heights, and free energy profiles are constructed to estimate the isomeric branching ratios of the degradation pathways, and thereby identify the dominant reaction channels and major products.

Computational Details

All geometry optimizations were performed using density functional theory (DFT) with Becke's three parameter hybrid method using the LYP correlation functional (B3LYP) in conjunction with the split valence polarized and diffuse basis set 6-31+G(d,p) as implemented in the GAUSSIAN 03 package.[24–27] The optimized isomers were examined with harmonic frequency calculations to confirm transition states and to obtain zero-point energy (ZPE) and thermal corrections. On B3LYP geometries, single-point calculations using BB1K, BMK, and MPW1K methods with cc-pVTZ basis sets were performed on some important structures for result section. The energies reported herein are potential energies from BMK results and corrected with ZPE contributions. For all first-order saddle points, intrinsic reaction coordinate (IRC) [28,29] calculations were performed revealing the geometries of the local minima in conjunction with a given transition state.

[a] S.-X. Hu, E. Y. Zeng
State Key Laboratory of Organic Geochemistry, Guangzhou Institute of Geochemistry, Chinese Academy of Sciences, Guangzhou 510640, China
[b] S.-X. Hu
Graduate School of the Chinese Academy of Sciences, Beijing 100049, China
[c] J.-G. Yu
College of Chemistry, Beijing Normal University, Beijing 100875, China
E-mail: jianguo_yu@bnu.edu.cn

Contract grant sponsors: National Natural Science Foundation of China; contract grant numbers: 41121063, 21073014.
Contract grant sponsor: Guangzhou Institute of Geochemistry, Chinese Academy of Sciences; contract grant number: GIGCAS 135 project Y234081001.

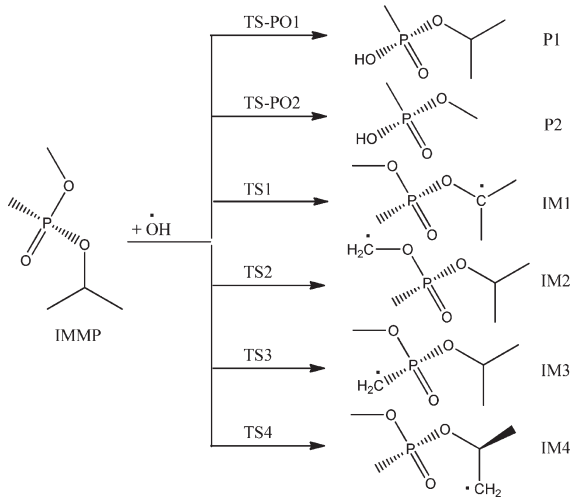

Figure 1. Initial reactions of IMMP and OH.

Results and Discussion

OH-initial degradation pathways of IMMP

It is well known that a hydroxyl radical has a strong nucleophilicity and can abstract H atoms from alkyls or substitute alkoxy groups in IMMP. The first reaction of hydroxyl radical and IMMP (Figure 1) forms a complex (RE, Figure 2) that is exothermic by 7.80 kcal/mol (Table 1 and Figure 3). Subsequent, H-abstraction may potentially occur at four alkyl positions (noted in RE as isopropyl C1 carbon, methyl C4, C5, and C2 carbons, Figure 2). Therefore, four transition states (TS1, TS2, TS3, and TS4) in the reactive routes are found corresponding to abstraction of the isopropyl H1 hydrogen, methyl H2, H14, and H3 hydrogens with energies 2.57, 3.90, 8.31, and 5.15 kcal/mol higher than that of RE. The formations of the corresponding products (IM1, IM2, IM3, and IM4) are exothermic by 13.23, 11.19, 5.85, and 5.49 kcal/mol, respectively. Thus, these relatively low energy barriers indicate that all four reactions can occur readily in the atmosphere.

In addition, the two alkoxy groups $(CH_3)_2CHO—$ and $CH_3O—$ attached to the P atom in IMMP could be substituted by OH radicals to form $CH_3OP(O)(CH_3)OH$ (P1) or $(CH_3)_2CHOP(O)(CH_3)OH$ (P2). For these two substitution channels, the optimized geometries of the products and corresponding transition states (TS–PO1 and TS–PO2) are obtained with barrier heights of 8.67 and 32.53 kcal/mol, respectively. These two reactions are also exothermic. Compared to the lower energy barriers for the H-abstraction channels, the $(CH_3)_2CHO—$ and $CH_3O—$ group substitutions are less favorable in this stepwise reaction (Table 1 and Figures 1–3).

With an energy barrier more than 10 times lower than those for alkoxy-substitution, H-abstraction channels are more significant in the reaction of IMMP with OH radicals than the alkoxyl-substitution channels. Conversely, a major product observed in the experimental study,[23] $CH_3OP(O)(CH_3)OH$ (molecular weight 138), is less likely to be produced in the first step due to an extremely high energy barrier, which is in agreement with a previous experimental conclusion that $(CH_3)_2CHOP(O)(CH_3)OH$ is formed via H-atom abstraction from the $—OCH_3$ group.[23]

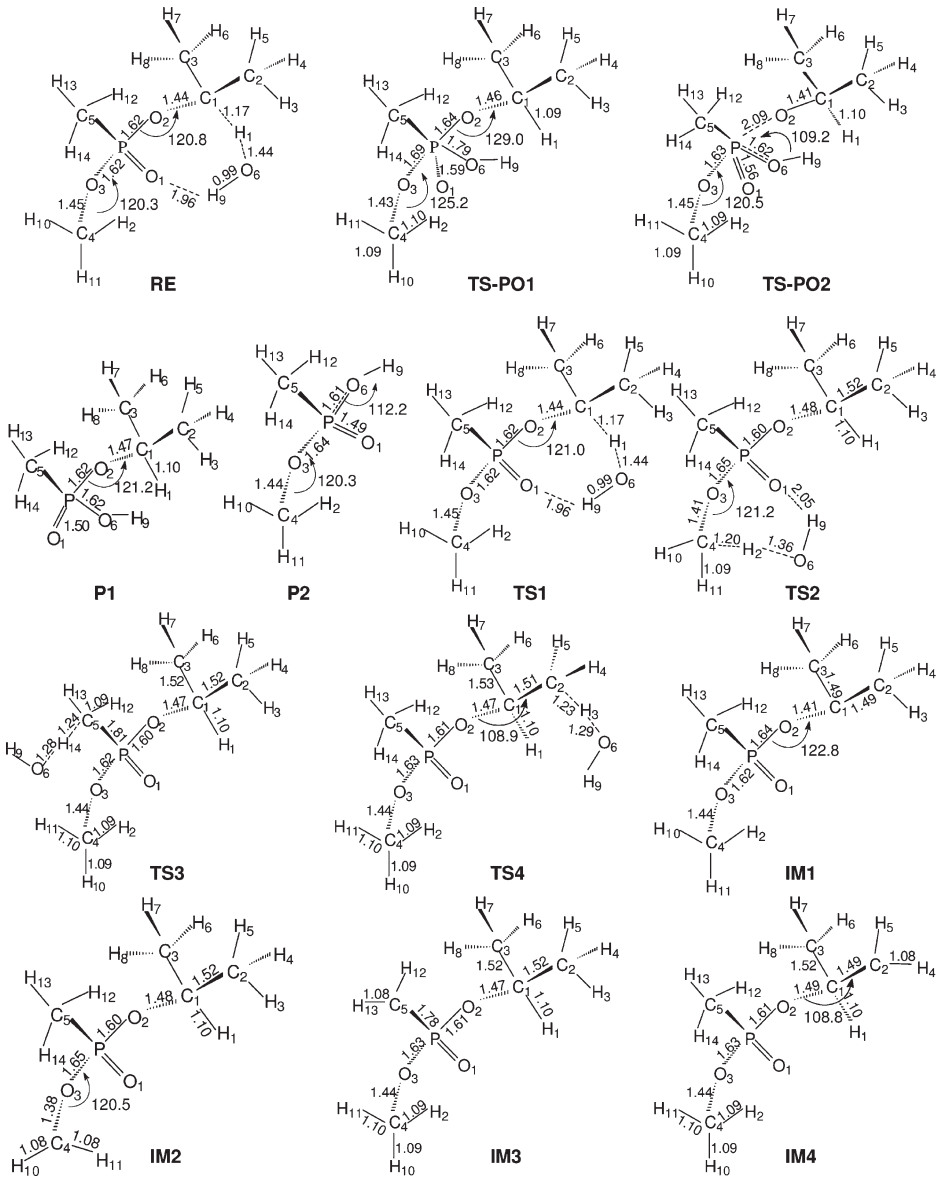

Figure 2. Optimized structures of investigated reactions of IMMP and OH radicals as obtained from B3LYP/6-31tG (d, p) calculation. For clarity, many bond lengths in the system are left out and are not shown in the figure. Distances are in angstroms, and angles are in degrees.

Table 1. Relative potential energy (ΔE^0) and relative Gibbs free energy (ΔG^0) for all the stationary points, activation potential energy (ΔE^*), activation Gibbs free energy (ΔG^*),and rate constants (K) at 298 K calculated for all barrier paths at the BMK/cc-pVTZ//B3LYP/6–31+G (d,p) level.

		$\Delta E^{*[b]}$			$\Delta G^{*[b]}$			K			$\Delta E^{0[b]}$			$\Delta G^{0[b]}$		
Reactions[a]	TS	ΔE_{bb1k}	ΔE_{bmk}	ΔE_{mpw1k}	ΔG_{bb1k}	ΔG_{bmk}	ΔG_{mpw1k}	K_{bb1k}	K_{bmk}	K_{mpw1k}	ΔE_{bb1k}	ΔE_{bmk}	ΔE_{mpw1k}	ΔG_{bb1k}	ΔG_{bmk}	ΔG_{mpw1k}
IMMP+OH-RE											−7.27	−7.80	−13.03	−0.17	−0.70	−5.93
RE-IM1+H_2O	ts1	3.67	2.57	4.99	5.31	3.67	0.86	3.29E-11[c]	5.2E-10[c]	5.96E-08[c]	−20.80	−21.04	−19.55	−21.89	−22.13	−20.64
RE-IM2+H_2O	ts2	5.03	3.90	6.52	6.48	4.82	2.21	4.49E-12[c]	7.48E-11[c]	6.14E-09[c]	−17.87	−18.99	−16.67	−18.42	−19.54	−17.21
RE-IM3+H_2O	ts3	9.31	8.31	10.84	10.43	8.90	6.20	5.69E-15[c]	7.65E-14[c]	7.24E-12[c]	−11.91	−13.65	−11.32	−13.21	−14.95	−12.63
RE-IM4+H_2O	ts4	6.60	5.15	7.48	8.08	6.10	3.20	3.02E-13[c]	8.54E-12[c]	1.15E-09[c]	−12.38	−13.29	−11.86	−13.6	−14.52	−13.09
RE-P1+ CH_3O	ts-po1	10.93	11.04	−15.00	11.84	11.41	10.15	5.26E-16[c]	1.09E-15[c]	9.24E-15[c]	−14.41	−14.51	−4.61	−16.59	−16.69	−6.79
RE-P2+C_3H_7O	ts-po2	35.85	34.24	40.58	38.05	35.90	37.01	3.19E-35[c]	1.19E-33[c]	1.83E-34[c]	−11.82	−12.11	33.3	−14.77	−15.06	15.98
IM1+O2-IM5											−29.63	−35.27	−26.49	−18.09	−23.73	−14.95
IM2+O2-IM6											−31.34	−35.54	−28.85	−21.03	−25.23	−18.54
IM3+O2-IM7											−22.54	−26.24	−19.57	−13.01	−16.71	−10.04
IM3+O2-IM8											−30.51	−35.22	−27.32	−20.18	−24.89	−16.98
IM5+NO-IM9+NO_2	ts5	33.62	31.88	33.47	43.71	41.97	28.61	2.25E-39[c]	4.25E-38[c]	2.66E-28[c]	−17.69	−15.7	−19.66	−18.55	−16.56	−35.46
IM6+NO-IM10+NO_2	ts6	30.01	28.6	29.51	39.93	38.53	20.89	1.33E-36[c]	1.42E-35[c]	1.22E-22[c]	−18.55	−15.88	−20.27	−19.53	−16.86	−39.79
IM7+NO-IM11+NO_2	ts7	30.68	28.74	30.46	41.28	39.34	31.03	1.35E-37[c]	3.59E-36[c]	4.45E-30[c]	−16.77	−14.39	−17.93	−17.11	−14.72	−28.30
IM8+NO-IM12+NO_2	ts8	30.88	29.37	30.37	40.66	31.42	23.16	3.88E-37[c]	2.33E-30[c]	2.63E-24[c]	−15.42	−12.93	−17.12	−15.75	−21.00	−34.44
IM5-P3	ts9	22.12	20.53	21.67	23.62	22.02	23.17	2.96E-05[d]	4.37E-04[d]	6.35E-05[d]	14.13	13.24	13.38	14.14	13.25	13.39
IM5-P4	ts10	27.11	26.11	26.36	29.00	27.99	28.25	3.37E-09[d]	1.82E-08[d]	1.19E-08[d]	18.89	17.82	17.25	19.84	18.77	18.20
IM6-P5	ts11	19.03	17.46	19.08	20.36	18.79	20.41	7.27E-03[d]	1.03E-01[d]	6.62E-03[d]	9.28	8.86	8.85	8.16	7.74	7.73
IM6-P6	ts12	27.58	26.38	27.04	30.04	28.84	29.50	5.76E-10[d]	4.38E-09[d]	1.43E-09[d]	19.15	17.87	17.53	20.36	19.08	18.75
IM9-P7+C_2H_6CO	ts13	22.78	21.3	26.22	22.51	21.03	25.94	1.92E-04[d]	2.35E-03[d]	5.84E-07[d]	13.06	12.53	44.49	−0.69	−1.22	30.74
IM9-P8+CH_3	ts14	12.71	10.72	14.39	12.52	10.53	14.19	4.10E+03[d]	1.18E+05[d]	2.43+E02[d]	−1.24	−2.84	−1.36	−12.76	−14.35	−12.88
IM10-P9+CHO	ts15	13.41	11.46	15.38	13.73	11.78	15.69	5.33E+02[d]	1.42E+04[d]	1.92E+01[d]	−1.75	−4.71	0.80	−12.58	−15.53	−10.02
IM10+O_2-P10+HO_2	ts16	12.37	8.97	14.93	21.70	18.29	24.26	3.10E-23[c]	9.79E-21[c]	4.15E-25[c]	−33.10	−38.50	−26.61	−34.16	−39.55	−27.66
IM12-P11+CH_2O	ts17	15.54	13.55	17.64	14.49	12.50	16.59	1.46E+02[d]	4.26E+03[d]	4.21[d]	13.34	11.71	15.38	1.02	−0.60	3.06

[a] IM and TS represent intermediate product and transition state, respectively. [b] Unit in kcal/mol. [c] Unit in kcal/mols^{-1}. [d] Unit in s^{-1}.

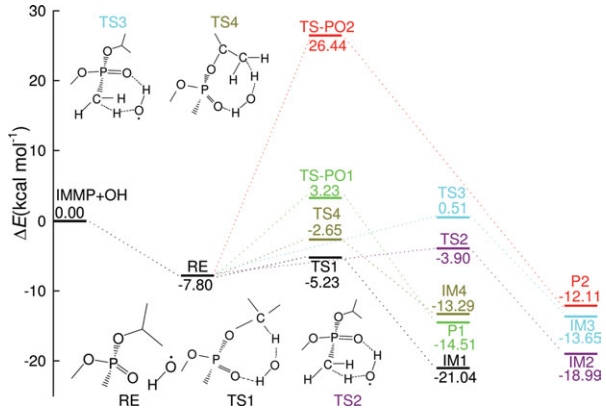

Figure 3. Relative energy, represented by the vertical axis, show potential energy profiles for the reaction paths of IMMP with OH radicals at the BMK/ cc-pVTZ level of theory with ZPE. [Color figure can be viewed in the online issue, which is available at wileyonlinelibrary.com.]

Atmospheric secondary reactions

It is well established that O_2-addition to alkyl radicals (·R) to form peroxy radicals (·RO_2) occurs readily in the troposphere.[30] Our calculations on the systems considered here show that O_2-addition forming the radicals of $(CH_3)_2C(O_2)OP(O)(CH_3)OCH_3$ (IM5), $(CH_3)_2CHOP(O)(CH_3)O(CH_2O_2)$ (IM6), $(CH_3)_2CHOP(O)(CH_2O_2)(OCH_3)$ (IM7), and $(CH_3)(CH_2O_2)CHOP(O)(CH_3)OCH_3$ (IM8) is a barrier free association and is exothermic by 35.27 and 35.54, 26.24, and 35.22 kcal/mol, respectively (Table 1 and Figures 4 and 5).

Reactions of peroxy radicals

Under atmospheric conditions, the reaction of peroxy radicals with atmospheric NO is observed experimentally and has been confirmed in several theoretical studies.[30] Reactions of different intermediates with NO are illustrated in Figure 4 and described herein in detail. Upon forming complex, IM5-NO directly dissociates into IM9 and NO_2 with simultaneous O4—O5 bond scission via a transition state (TS5) with an energetic requirement of 31.88 kcal/mol. The calculated exothermicity of 15.70 kcal/mol shows that this process occurs readily in the atmosphere. The critical C1—O4 bond is shortened from 1.50 Å in IM5 and 1.45 Å in TS5 to 1.34 Å in IM9. For IM6, upon forming IM6–NO complex, cleavage of the O4—O5 bond yields $(CH_3)_2CHOP(O)(CH_3)O(CH_2)O$ (IM10) and NO_2 via the transition state TS6 with an energy barrier of 28.60 kcal/mol. In IM10, the length of the C4—O4 bond is shortened to 1.33 Å from 1.46 Å in IM6. This process is strongly exothermic by 15.88 kcal/mol. Similarly, the rapid reaction of IM7/IM8 radicals with NO to form IM11/IM12 + NO_2 can proceed via the transition states, TS7 and TS8. These two paths are exothermic by 14.39 and 12.93 kcal/mol with energy barriers of 28.74 and 29.37 kcal/mol, respectively. In IM11, the C5—O4 length shows double bond-like characteristics similar to IM9 with a bond length of 1.34 Å, which is shortened from 1.45 Å in IM7 and 1.43 Å in TS1. In IM12, the length of the C2—O5 bond is 1.36 Å, indicating a strong carbon oxygen bond (Table 1 and Figures 5 and 6).

Additionally, peroxy radicals (·RO_2) are believed to be removed through H-rearrangements in the atmosphere. There are two possible H-rearrangement procedures for IM5 (Figure 7). For the first path, H2 shifts from C4 atom in the CH_3O— group to O5 atom via TS9, an eight-member transition state. The IRC calculation shows that $(CH_3)_2C(O_2H)OP(O)(CH_3)OCH_2$ (P3) is connected to TS9 in the forward direction, and the corresponding barrier height is 20.53 kcal/mol on the potential energy profile. For the other H-rearrangement path, the calculated transition vector (imaginary frequency of 1495i cm^{-1}) clearly shows the motion of H12 between C5 atom in —CH_3

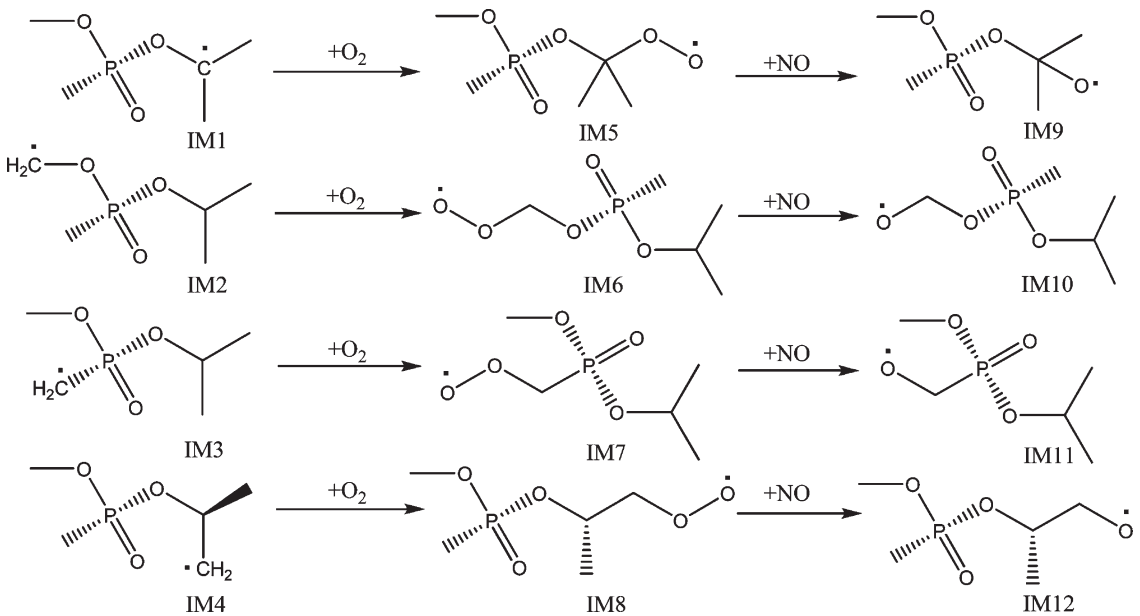

Figure 4. Oxidation of intermediates (IM1, IM2, IM3, and IM4) under the present of O_2/NO.

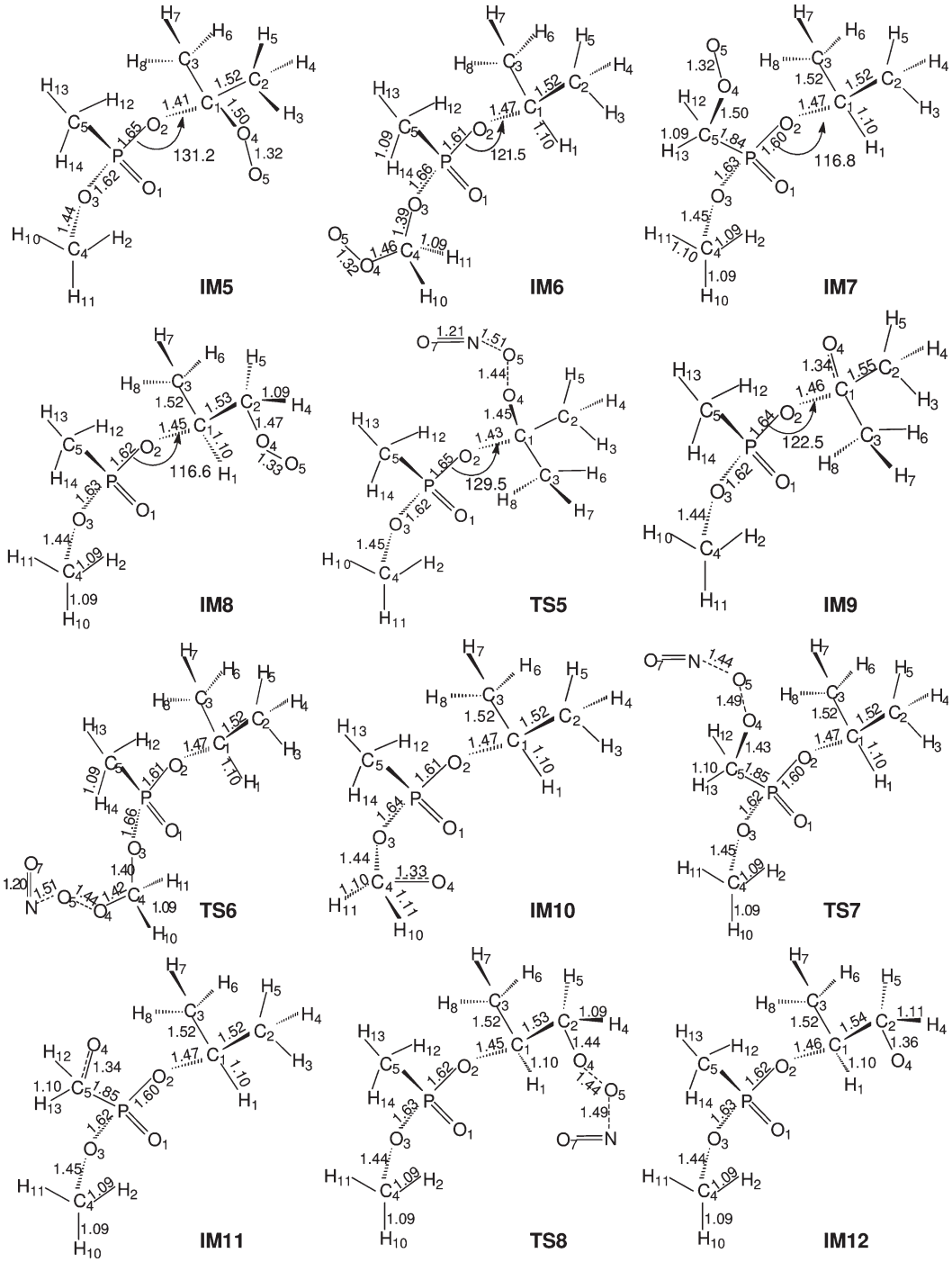

Figure 5. Structures of the reactions of intermediate radicals and O2/NO as obtained at B3LYP/6-31tG(d,p) level of theory. Distances are in angstroms, and angles are in degrees.

group and the terminal O5 via TS10 with an energy barrier of about 26.11 kcal/mol. Downhill, $(CH_3)_2C(O_2H)OP(O)(CH_2)OCH_3$ (P4) is generated. In P4, the length of 0.97 Å for the H12—O5 bond shows that H12 attaches to O5 with both C1—O4 and P—C5 bond lengths reduced by 0.02 Å from 1.79 and 1.44 Å, respectively, in TS10. The endothermicity of these two paths with energetic demands of 13.24 and 17.82 kcal/mol indicates the instability of the hydroperoxides produced in this system. Similar to H-migration for IM5, two H-migration channels for IM6 are also considered (Figure 7). Both channels are endothermic and require energies of 8.86 and 17.86 kcal/mol to yield hydroxperoxide radicals P5 and P6, respectively. Their corresponding transition states (TS11 and TS12) are 17.45 and 26.38 kcal/mol higher than IM6 in energy (Table 1 and Figures 8 and 9).

Reactions of IM9, IM10, and IM12

Subsequent degradation from IM9 involves two unimolecular decomposition channels (Figure 10). One removal pathway of IM9 via TS13 involves cleavage of the C1—O2 bond to form

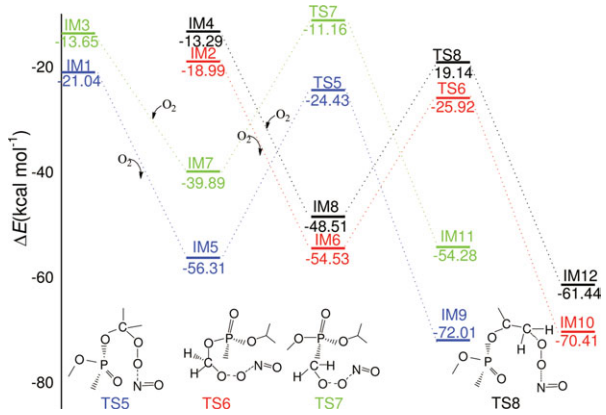

Figure 6. Potential energy profiles for the degradation pathways of alkyls in the presence of O_2/NO at the BMK/ cc-pVTZ level of theory with ZPE. [Color figure can be viewed in the online issue, which is available at wileyonlinelibrary.com.]

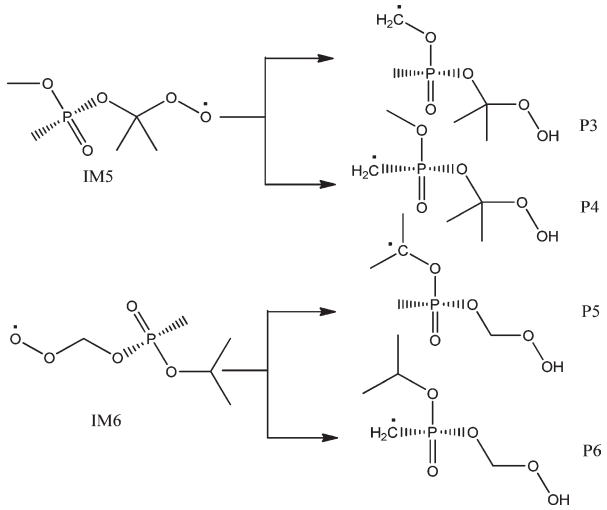

Figure 7. Formation of hydroperoxides according to H-rearrangement from peroxy radicals (IM5 and IM6).

$CH_3OP(O)(CH_3)O$ (P7) and molecular acetone. This process has an apparent barrier of 23.95 kcal/mol and is endothermic by 15.69 kcal/mol. In P7, the P—O2 bond is reduced from 1.64 Å in IM9. No other obvious geometric changes between IM9 and P7 are observed. The other decomposition pathway to produce a $CH_3OP(O)(CH_3)OC(O)CH_3$ radical (P8) and a CH_3 radical,

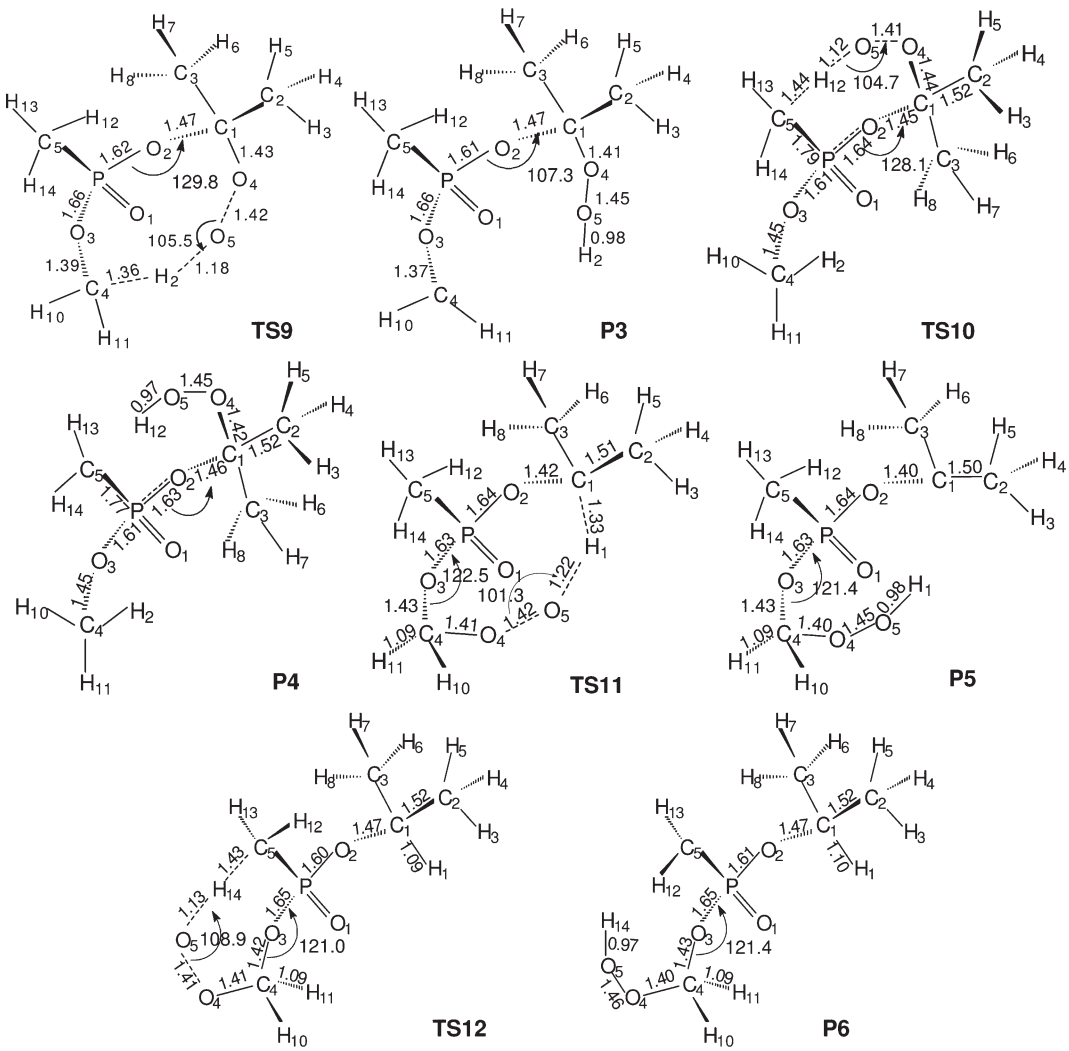

Figure 8. Optimized geometries of the transition states and products involved in the reaction of H-rearrangement at B3LYP/6-31tG (d,p) level of theory. Distances are in angstroms, and angles are in degrees.

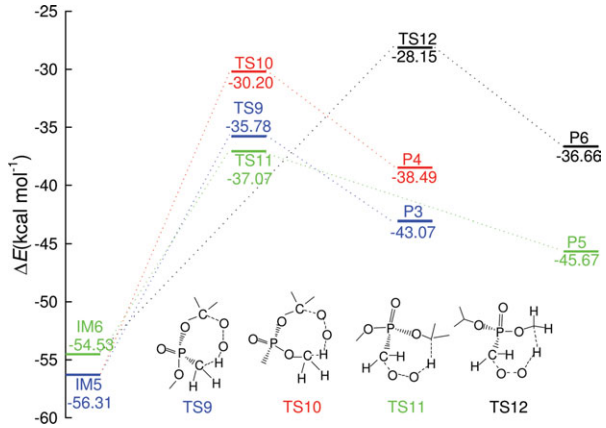

Figure 9. Potential energy profiles for the H -rearrangement channels of IM5 and IM6 at the BMK/cc-pVTZ level of theory with ZPE. [Color figure can be viewed in the online issue, which is available at wileyonlinelibrary.com.]

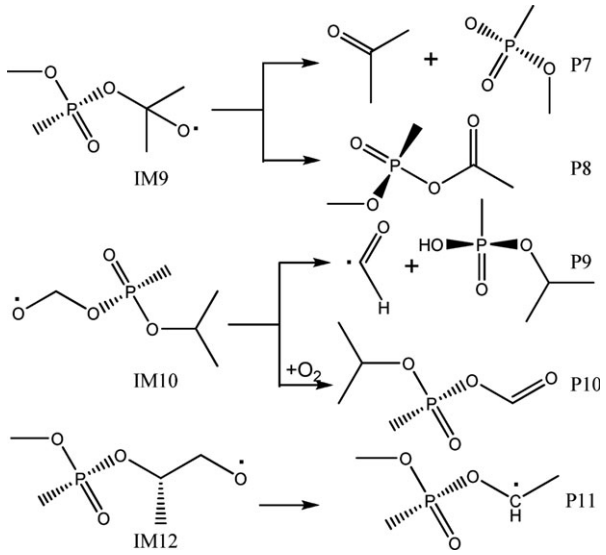

Figure 10. Degradation mechanism of secondary reactants (IM9, IM10, and IM12) to their related products upon oxidation.

a dominant product observed experimentally,[23] is through a direct fission of the C1—C2 bond. The formation of P8 is identified to be endothermic by 3.67 kcal/mol via the transition state TS14 in this study. This reaction surmounts a relatively low energy barrier of 9.92 kcal/mol in comparison to the H-rearrangement paths. Further removal of CH_3 radicals with atmospheric O_2 would lead to the formation of CO.[21,23] In P8,

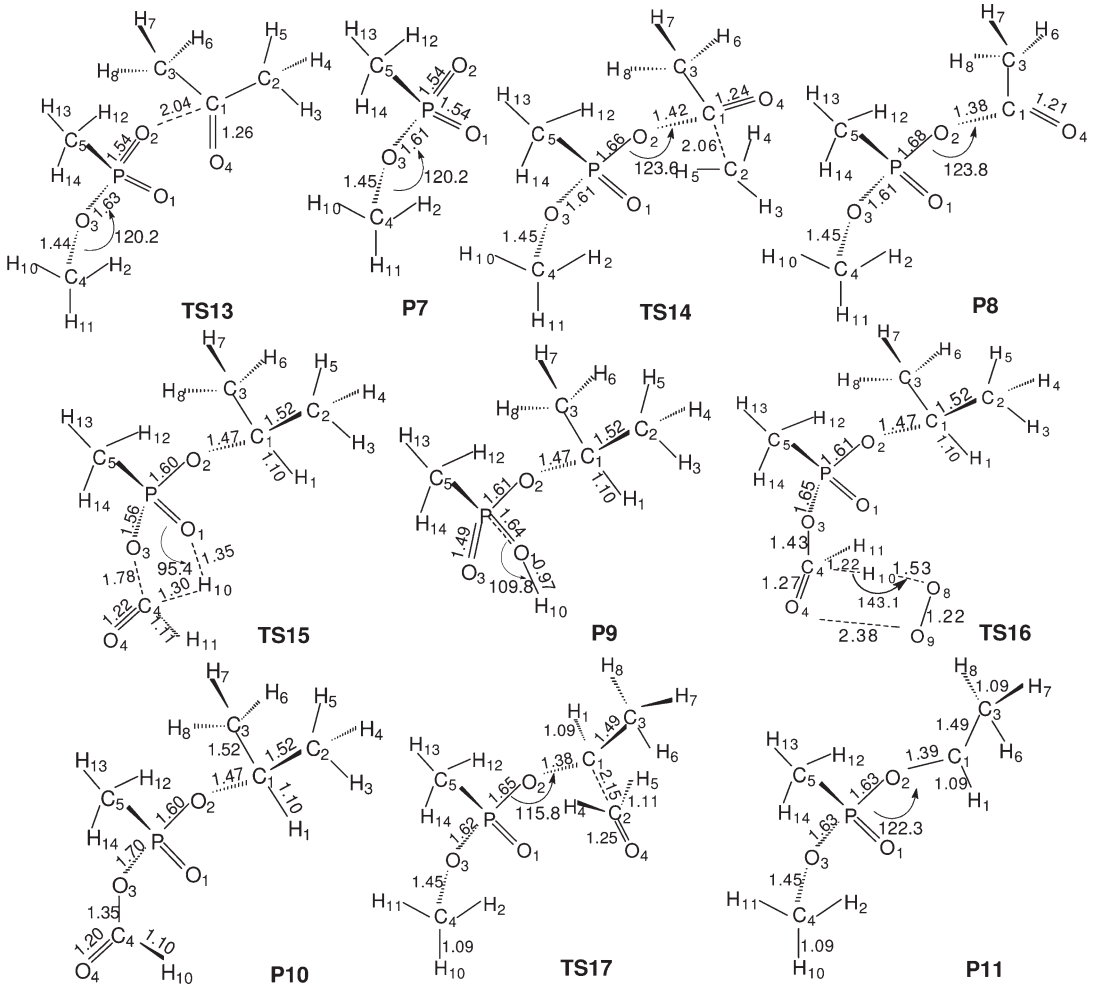

Figure 11. Optimized geometries of the transition states and products involved in the reaction of IM9, IM10, and IM12 at B3LYP/6-31tG(d, p) level of theory. Distances are in angstroms, and angles are in degrees.

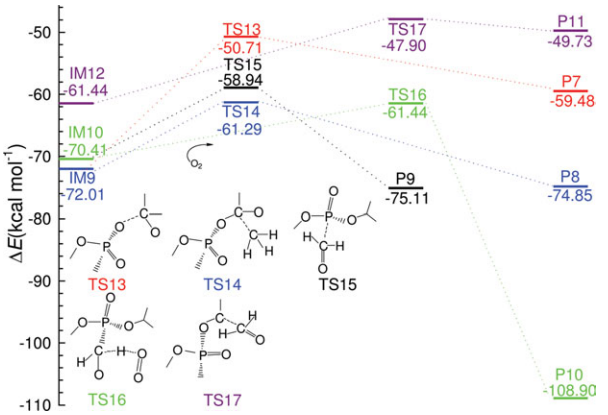

Figure 12. Potential energy profiles for the formation routes of degradable products at the BMK/ cc-pVTZ level of theory with ZPE. [Color figure can be viewed in the online issue, which is available at wileyonlinelibrary.com.]

the lengths of C1—O2 and C1—O4 bonds are shortened by 0.08 and 0.13 Å compared to IM9. For both of these dissociation processes, no five-membered transition state and no products of the >P(O)OH and carbonyl radical are found. This provides evidence that different mechanisms are responsible for degradation of OPs containing —OCH_3 or —OCH_2— groups and —$OCH(CH)_3$ groups. The energy required for scission of the C1—O2 bond is less than that for cleavage of the C1—C2 bond, indicating that the former pathway can be attributed to the dominant degradation of IM9 (Figures 11 and 12).

Further reactions of IM10 are predicted to be unimolecular dissociation or reaction with O_2 (Figure 10). In the dissociation process, $(CH_3)_2CHOP(O)(CH_3)OH$ (P9) which was reported in a previous experimental study,[23] can be formed via a five-centered transition state (TS15) by in this study. This result is consistent with a previous theoretical study that >P(O)—OCH_2O radical passes through a five-member transition state to form >P(O)OH and a molecular carbonyl radical.[21] Cleavage of the C4—O3 bond and H10 atom migration onto O1 requires an energy barrier of around 11.46 kcal/mol and consequent the formation of P9 is exothermic by 4.71 kcal/mol. In P9, the P—O3 distance is shortened to 1.50 Å from 1.64 Å in IM10, while the length of the newly formed H10—O1 bond is reduced to 0.99 Å. In another removal pathway, the reaction of alkoxy radical (IM10) and O_2 was predicted to be significant in the degradation of alkoxyl radicals in the troposphere by Atkinson.[12,30] The reaction of IM10 and O_2 is computed to be an exothermic process by 38.50 kcal/mol, with an energy barrier of 8.97 kcal/mol according to the energy profiles presented in Figure 12. The encounter transition state (TS16) where O_2^+ interacts at distance of 2.38 and of 1.53 Å with the oxygen atom and the hydrogen atom of carbonyl group, respectively. The transition state TS16 easily isomerizes to a molecular HO_2 radical and product P10 where the bond length for carbon and oxygen is 1.20 Å in the newly formed aldehyde group. Because of those two relatively feasible energy barriers, the formations of stable products are able to occur competitively. This result contradicts observations from the experimental paper[23] where no experimental observation of weight 166 was reported (Table 1 and Figures 11 and 12).

Additionally, the removal of IM12 could occur by unimolecular dissociation and the formation of (CH3CHO)P(O)(-CH3)(OCH3) (P11) and molecular formaldehyde (Figure 10). This process is endothermic by 11.71 kcal/mol with a free energy barrier of 13.55 kcal/mol. For the corresponding transition state (TS17), the length of the C1—C2 carbon bond and the angle of P—O2—C1 are 2.15 Å and 122.48° which are extended from 1.54 Å and 120.53° in IM12, respectively (Table 1 and Figures 11 and 12).

Conclusions

Results from DFT show that the formation of IM1 is the favored pathway of the for competitive H-abstraction pathways considered here. In all pathways, the rate-determining step was found to be the formation of IM1/IM2/IM3/IM4 from isolated reactants (IMMP and OH radical). Moreover, $(CH_3)_2CHOP(O)(CH_3)OH$ is confirmed to be generated in secondary reactions of IMMP, as suggested in the experimental paper.[23] In addition, we suggest that the experimentally unreported compound, $CH_3OP(O)(CH_3)OC(O)CH_3$ with molecular weight 166, can be formed by the reaction of $(CH_3)_2CHOP(O)(CH_3)O(CH_2O)$ (IM10) and O_2. The negative effects of these degradation products on the environment and human health require further experimental and theoretical investigation.

Acknowledgments

This is contribution No. IS–1503 from GIGACS.

Keywords: isopropyl methyl methylphosphonate · density functional theory · degradation mechanism · reaction channel · rate constant

How to cite this article: S.-X. Hu, J.-G. Yu, E. Y. Zeng, *Int. J. Quantum Chem.* **2013,** *113*, 1128–1136. DOI: 10.1002/qua.24182

Additional Supporting Information may be found in the online version of this article.

[1] H. D. Burrows, L. M. Canle, J. A. Santaballa, S. Steenken, *J. Photochem. Photobiol. B Biol.* **2002**, *67,* 71.
[2] Y. Yao, T. Harner, P. Blanchard, L. Tuduri, D. Waite, L. Poissant, C. Murphy, W. Belzer, F. Aulagnier, E. Sverko, *Environ. Sci. Technol.* **2008**, *42,* 5931.
[3] D. E. Glotfelty, M. S. Majewski, J. N. Selbert, *Environ. Sci. Technol.* **1990**, *24,* 353.
[4] S. O. Pehkonen, Q. Zhang, *Crit. Rev. Environ. Sci. Technol.* **2002**, *32,* 17.
[5] J. G. Ekerdt, K. J. Klabunde, J. R. Shapley, J. M. White, J. T. Yates, *J. Phys. Chem.* **1988**, *92,* 6182.
[6] K. Jaga, C. Dharmani, *Pan Am. J. Public Health* **2003**, *14,* 171.
[7] F. van den Berg, R. Kubiak, W. G. Benjey, M. S. Majewski, S. R. Yates, G. L. Reeves, J. H. Smelt, van der A. M. A. Linden, *Water Air Soil Pollut.* **1999**, *115,* 195.
[8] R. H. Coupe, M. A. Manning, W. T. Foreman, D. A. Goolsby, M. S. Majewski, *Sci. Total Environ.* **2000**, *248,* 227.

[9] T. E. Bidleman, *Environ. Sci. Technol.* **1988**, *22,* 361.
[10] N. B. Munro, S. S. Talmage, G. D. Griffin, L. C. Waters, A. P. Watson, J. F. King, V. Hauschild, *Environ. Health Perspect.* **1999**, *107,* 933.
[11] P. Martin, E. C. Tuazon, R. Atkinson, A. D. Maughan, *J. Phys Chem. A* **2002**, 106, 1542.
[12] R. Atkinson, S. M. Aschmann, M. A. Goodman, A. M. Winer, *Int. J. Chem. Kinet.* **1988**, *20,* 273.
[13] E. C. Tuazon, R. Atkinson, S. M. Aschmann, J. Arey, A. M. Winer, J. N. Pitts, Jr., *Environ. Sci. Technol.* **1986**, *20,* 1043.
[14] M. A. Goodman, S. M. Aschmann, R. Atkinson, A. M. Winer, *Arch Environ. Contam. Toxicol.* **1988**, *17,* 281.
[15] M. A. Goodman, S. M. Aschmann, R. Atkinson, A. M. Winer, *Environ. Sci. Technol.* **1988**, *22,* 578.
[16] J. K. Parker, C. Espada-Jallad, *J. Phys. Chem. A* **2009**, *113,* 9814.
[17] S. M. Aschmann, E. C. Tuazon, R. Atkinson, *J. Phys. Chem. A* **2005**, *109,* 11828.
[18] R. T. Rewick, M. L. Schumacher, D. L. Haynes, *Appl. Spectrosc.* **1986**, *40,* 152.
[19] Q. Zhou, X. Shi, F. Xu, Q. Zhang, M. He, W. Wang, *Atmos. Environ.* **2009**, *43,* 4163.
[20] Q. Zhou, X. Sun, R. Gao, Q. Zhang, W. Wang, *J. Mol. Struct. (Theochem)* **2010**, *952,* 8.
[21] Q. Zhang, X. Qu, W. Wang, *Environ. Sci. Technol.* **2007**, *41,* 6109.
[22] S. M. Aschmann, W. D. Long, R. Atkinson, *J. Phys. Chem. A* **2008**, *112,* 4793.
[23] S. M. Aschmann, E. C. Tuazon, W. D. Long, R. Atkinson, *J. Phys. Chem. A* **2010**, *114,* 3523.
[24] C. Lee, W. Yang, R. G. Parr, *Phys. Rev. B Condensed Matter Mater. Phys.* **1988**, *37,* 785.
[25] A. D. Becke, *J. Chem. Phys.* **1993**, *98,* 5648.
[26] L. A. Curtiss, K. Raghavachari, P. C. Redfern, J. A. Pople, *J. Chem. Phys.* **1997**, *106,* 1063.
[27] M. J. Frisch, G. W. Trucks, H. B. Schlegel, G. E. Scuseria, M. A. Rob, J. R. Cheeseman, J. A. Montgomery Jr., T. Vreven, K. N. Kudin, J. C. Burant, J. M. Millam, S. S. Iyengar, J. Tomasi, V. Barone, B. Mennucci, M. Cossi, G. Scalmani, N. Rega, G. A. Petersson, H. Nakatsuji, M. Hada, M. Ehara, K. Toyota, R. Fukuda, J. Hasegawa, M. Ishida, T. Nakajima, Y. Honda, O. Kitao, H. Nakai, M. Klene, X. Li, J. E. Knox, H. P. Hratchian, J. B. Cross, C. Adamo, J. Jaramillo, R. Gomperts, R. E. Stratmann, O. Yazyev, A. J. Austin, R. Cammi, C. Pomelli, J. W. Ochterski, P. Y. Ayala, K. Morokuma, G. A. Voth, P. Salvador, J. J. Dannenberg, V. G. Zakrzewski, S. Dapprich, A. D. Daniels, M. C. Strain, O. Farkas, D. K. Malick, A. D. Rabuck, K. Raghavachari, J. B. Foresman, J. V. Ortiz, Q. Cui, A. G. Baboul, S. Clifford, J. Cioslowski, B. B. Stefanov, G. Liu, A. Liashenko, P. Piskorz, I. Komaromi, R. L. Martin, D. J. Fox, T. Keith, Al-M. A. Laham, C. Y. Peng, A. Nanayakkara, M. Challacombe, P. M. W. Gill, B. Johnson, W. Chen, M. W. Wong, C. Gonzalez, J. A. Pople, Gaussian, Inc.: Wallingford, CT, **2003**.
[28] C. Gonzalez, H. B. Schlegel, *J. Chem. Phys.* **1989**, *90,* 2154.
[29] K. Fukui, *Acc. Chem. Res.* **1981**, *14,* 363.
[30] R. Atkinson, *Atmos. Environ.* **2000**, *34,* 2063.

Received: 17 January 2012
Revised: 29 April 2012
Accepted: 30 April 2012
Published online on 5 June 2012